A comprehensive anatomical characterization and radiographic study of stage III testicular cancer in a 31-year-old male patient

Ernest F. Talarico, Jr.[1A], Jose L. Mas[1A] and Jonathan A. Jones[2B]

[1]*Anatomy & Cell Biology,* [2]*Family Medicine Residency Program,* [A]*Indiana University School of Medicine-Northwest, Gary, Indiana,* [B]*Union Hospital, Terre Haute, Indiana*

SUMMARY

The purpose of this investigation was to characterize an unusual case of stage III testicular germ cell tumor (TGCT) in a 31-year-old male with metastases to nodes, bone, viscera and brain, and to understand all possible routes of metastatic disease. Testicular cancer (TC) has an increasing incidence worldwide, and its etiology, risk factors and pathogenesis are not completely understood. Medical records were reviewed, and the cadaveric specimen evaluated by physical examination and gross dissection. Paraffin embedded tissue sections of the primary tumor were stained with Hematoxylin and Eosin (H&E) for histological study. To examine metastatic spread, pre- and post-mortem digital radiologic image acquisition was done using x-ray films, and high- resolution CT Scans and MRI Scans. Image analysis, multiplanar reformatting, and three- dimensional (3-D) reconstruction were done on radiographic series. Dissection showed masses bilaterally from the apex through the lung base; masses on the internal thoracic wall, and hepatomegaly and splenomegaly with multiple tumor masses. Testicular parenchyma was composed of primitive germ cells that formed glomeruloid or embryonal-like structures, as well as areas with a micro-cystic histologic pattern and areas of fibrous dysplasia. Medical imaging 3- D video radiographic dissection was notable for a 38.45 mm diameter, mid-brain tumor; extreme hepatomegaly with numerous tumors, lung tumors, a large penetrating tumor of the left ilium, and multiple tumors throughout both lungs and the thoracolumbar spine (T5-S1). This study provides insight into the histology and metastatic spread of TGCT that is essential for clinicians to understand in the evaluation and treatment of TC patients.

Key words: Testicular cancer – Germ cell tumor – Yolk sac tumor – Metastasis – Testicle – Brain

Abbreviations:
  Alpha-fetoprotein (AFP) Anterior-Posterior (AP)
  Autism Spectrum Disorder (ASD) Axial (AX)
  Bleomycin, Eetoposide and Cisplatin (BEP chemotherapy) Brain metastases (BM)
  Central Nervous System (CNS) Chest X-Ray (CXR)
  Computed Tomography (CT) Coronal (COR) Diethylstilbestrol (DES)
  Digital Imaging and Communications in Medicine (DICOM) Epithelial-Mesenchymal Transition (EMT)
  Etoposide, Ifosfamide and Cisplatin (VIP chemotherapy) Hematoxylin and Eosin (H&E)
  Indiana University School of Medicine — Northwest Campus (IUSM-NW) Inferior Vena Cava (IVC)
  Intervertebral (IV) Left (Lt)

Corresponding author: Ernest F. Talarico, Jr., Ph.D. Anatomy & Cell Biology, Site Director for Human Structure, Indiana University School of Medicine-Northwest, Dunes Medical Professional Building, Room 3028A, 3400 Broadway, Gary, Indiana 46408-1197, USA. Phone: 219-981-4356; Fax: 219-980-6566. E-mail: etalaric@iun.edu

Lumbar (L)
Magnetic Resonance Imaging (MRI) Multi-planar reformatting (MPR)
Retroperitoneal lymph node dissection (RPLND) Retroperitoneum (RP)
Right (R) Sagittal (SAG)
Testicular Cancer (TC)
Testicular Dysgenesis Syndrome (TDS) Testicular Germ Cell Tumor (TGCT) Thoracic (T)
Three-dimensional (3-D) United States (U.S.) Weighted (Wtd)
Yolk Sac Tumor (YST) Yolk Sack (YS)

INTRODUCTON

Testicular cancer (TC) is defined as a malignant neoplasm of the male sex organ (i.e., testicle). Although TC accounts for 1% of all male cancers (Trabert et al., 2015; Ferlay et al., 2013; Stevenson and Lowrance, 2015), it is the most common neoplasm among young men between 15-40 years of age (Trabert et al., 2015; Ferlay et al., 2013; McGlynn and Trabert, 2012; Ghazerian et al., 2015). Approximately 98% of all TCs are testicular germ cell tumors (TGCTs) (McGlynn and Trabert, 2012; Chia et al., 2010), and are histologically classified as seminoma, embryonal carcinoma, yolk sack tumor (YST), teratoma or choriocarcinoma (Choueiri et al., 2007; Ghazarian et al., 2015; National Cancer Institute PDQ®, 2017). Other types (i.e., non-TGCTs) include lymphomas, and those arising from Sertoli and Leydig cells. Among the TGCTs, one the most interesting is the YST, or endodermal sinus tumor, which is the most common TC in infants and young children, up to 4-years of age (Lotan, 2015; Talerman, 1980; Looijenga and Oosterhuis, 1999). In adults, this pure form of tumor is rare; instead, yolk sack (YS) elements frequently occur in combination with embryonal carcinoma making detection of adult YST difficult depending upon the amount of material available for pathologic studies and how the tissue sample is obtained (i.e., wedge vs. needle biopsy). However, recent studies linking the production of alpha- fetoprotein (AFP) with the presence of YST elements within a tumor complex demonstrate that AFP is a very useful marker for the presence of YST and emphasizes the importance of recognition and detection of elements (Stevenson and Lowrance, 2015; Milose et al., 2012; Talerman, 1980).

Over the past 40 years, the incident of TGCTs in developed countries has steadily risen (Vasdev et al. 2013; Suleymann et al., 2015; Chia et al., 2010; Trabert et al., 2015). Male Scandinavians, in particular from Norway and Denmark, have the highest incidence of TC worldwide (McGlynn and Trabert, 2012; Chia et al., 2010). Even further, the incidence of TGCTs in the United States (U.S.) is notably higher among Caucasian men than any other ethnicity (Hanna and Einhorn, 2014). In contrast, incidence rates are very low in Asia and Africa. In fact, incidence among African American patients is 1/5th the rate of white men in the U.S. Current studies indicate that TGCT incidence is increasing most rapidly among U.S. Hispanic males (Ghazarian et al., 2015). The median age for new cases is 34, where the incidence peaks between the ages of 20-40 and then declines greatly after age 50.

Research has suggested risk factors that include genetics, environment, recreational drug use and occupation (Cook et al., 2009, 2010; Hanna and Einhorn, 2014; Gurney et al., 2015). Risk is 8-10 times as high in a brother of a person with TC and 4-6 times as high in a son of a person with TC (Hanna and Einhorn, 2014). Other risk factors that seem to play a role in TC include diethylstilbestrol (DES) exposure, increased height, chemical exposure and HIV/AIDs. However, cryptorchidism is the most well characterized risk factor for TC (Cook et al., 2010; Pettersson et al., 2007; Rajpert-De Meyts et al., 2013), and TC is 10-40 fold higher in cryptorchidic testes. It is anticipated that 12% of all TGCTs arise in cryptorchid testes (Friedlander et al., 2015; Pettersson et al., 2007). Genetic disorders such as Down's syndrome and Testicular Dysgenesis Syndrome (TDS) are also associated with increased risk (Skakkebaek et al., 2001, 2003; Skakkaebaek et al., 2007; Ferguson and Agoulnik, 2013). In recent years, mutations of loci on chromosome 12q21 have been identified and suggested to be associated with TGCTs (Adra and Einhorn, 2017; Sheikine et al., 2012; Hanna and Einhorn, 2014; Elzinga-Tinke et al., 2015).

The most common site for metastasis in TC is the lymph nodes in the abdomen, but metastasis to the lung, liver, bones and brain can also occur (Feldman et al., 2016; Beard et al., 2015; Nagasawa et al., 2015; Boyle et al., 2013). This suggests multiple metastatic routes including hematogenous, lymphatic and direct invasion. Men with brain metastases (BM), either at initial diagnosis or metachronous at relapse, have a poor overall survival (Feldman et al., 2016). Even further, because BM of TGCTs are rare, the best method for medical management remains uncertain (Forquer et al., 2007; Boyle et al., 2013; Beyer et al., 2013). The survivors of TC are not only at risk of reoccurrence, but also at increased risk for metabolic syndrome, cardiovascular disease, nephrotoxic effects, psychosocial disorders, hypogonandism, fatigue, depression, osteoporosis and retrograde ejaculation (Hanna and Einhorn, 2014). Thus, because of the aggressiveness of TGCTs and their increasing incidence, a more comprehensive understanding of TGCTs is needed to so that clinicians can better diagnose, treat and manage patients. The present report investigates the unusual case of a 31-year-old male with stage III TGCT and metastases to nodes, bone, viscera and a large brain tumor, while utilizing imaging technology to better charac-

terize this disorder correlated to a survey of the current literature and a detailed review of routes of metastasis.

MATERIALS AND METHODS

Cadaveric Specimen

This study was conducted on a 31-year-old, white male cadaver as part of the International Human Cadaver Prosection Program and the formal course of human gross anatomy, both at the Indiana University School of Medicine - Northwest Campus (IUSM-NW; Gary, IN). With consent of this anatomical donor's family and with authorization of the State of Indiana Anatomical Education Program, medical and hospital records and tissue slides/blocks of the donor were acquired. Additional history (i.e., secondary medical history) was obtained through structured interviews with the maternal parent of this donor. All federal and state guidelines were followed regarding the use and care of cadaveric materials, as well as all regulations set forth by the State of Indiana Anatomical Education Program.

The embalming procedure is a 2-phase procedure beginning within the first 24 hours after death. The first step of the first phase of the embalming procedure is a mixture of 16 ounces of a 23 index (% Formaldehyde) embalming fluid and 16 ounces of a 25 index embalming fluid in 352 ounces of water. The overall index of this solution is 2.18. The second step is a mixture of 16 ounces of a 25 index embalming fluid in 176 ounces of water. The overall index of this solution is 2.27. Both mixtures are injected arterially using the right femoral artery. Drainage is by way of the femoral vein. After 48 hours, the second phase is a mixture of 16 ounces of a 30 index embalming fluid and 368 ounces of "EB Fluid" – a combination of Formalin, Phenol and Alcohol – also injected arterially using the right femoral artery. The specimen is then placed in a vat containing 9 gallons of 99% phenol solution, 6 gallons of 95% alcohol solution and 1500 gallons of water. The specimen remains submerged in the vat for a minimum of 4 months.

Gross Examination and Photography

Detailed physical examination was performed utilizing a "donor report", which is similar to an autopsy report, where gross observations and quantitative data were collected (Talarico, 2010, 2013). Digital photography of the external features and thoracic viscera was done using a NIKON D3100 SLR Camera (B&H Foto & Electronic Corporation, NY) equipped with an 18-55 mm VR NIKKOR Macro lens and a Nikon 40 mm f/2.8G AF-S DX NIKKOR 2200 VR Micro lens.

X-Ray Film Imaging

Plain x-ray imaging was performed in the radiology suite located on the second floor of the Dunes Medical Professional Building of the IUSM-NW. The following plain films were obtained: (1) anterior-posterior (AP) chest; (2) AP abdominopelvic; (3) upper extremity (pectoral girdle, brachium, antebrachium and carpus/manus); (4) lower extremity (pelvic girdle, thigh, leg and foot); (5) AP skull and lateral (Lat) skull.

Advanced Medical Imaging

Full-body, high-resolution CT and MRI imaging was completed at Methodist Hospitals Southlake Campus (Merrillville, IN) using a 64-slice CT scanner (General Electric Lightspeed® capable of 3-D reconstruction, and an MRI scanner (General Electric HIGH Speed MRI). Coronal (COR; frontal), axial (AX; transverse) and sagittal (SAG; median) views were generated both digitally and on film. Additional MRI scans included: (a) MRI of the brain including T1-weighted (Wtd) axial and sagittal; T2-Wtd axial, axial diffusion, and FLAIR axial scans; (b) MRI of the abdomen and pelvis to include T1- and T2-Wtd sequences in coronal and axial planes; (c) MRI of the knees, hips, and shoulders to consist of T1-, T2-Wtd, and STIR images in at least two planes; (d) MRI of the entire spine including T1- and T2-Wtd sagittal images.

Image Analysis

Processing of images, creations of 3D-reconstructions, and quantitative image analysis were done using Konicia PDI Viewer 1.00 V1.0R0.00 (KONICA Minolta, Ramsey, NJ) and TDK CDRS Dashboard V1.0.0.5 (TDK Medical, Minneapolis, MN) for digital x-ray films; eFILMTM LiteTM Viewer 3.0 (Merge Healthcare, Chicago, IL) for radiographic series from CT-Scans; and Philips iSite Viewer (Philips iSite, Amsterdam, Netherlands) for radiographic series from MRI Scans. Additional image analysis and reconstruction-reformatting was done using PACSGEAR (Perceptive Software, Pleasanton, CA) on radiographic series from CT scans and MRI scans. Multi-planar reformatting (MPR) was used to view slices in different planes for further analysis and measurement.

Video Clips

BodyViz® Interactive Anatomy Software Version 5.0 (Clive, IA) was used with Digital Imaging and Communications in Medicine (DICOM) data files from CT and MRI scans of the patient to construct high-resolution, 3-D images and video clips, as well as freeze-frame images. Tumor masses were measured and analyzed using video clips.

HISTORY

The patient is a 31-year-old white male, who died in 2013 secondary to Stage III Germ Cell TC (i.e., a rare adult form of TC as YST).

The patient presented to the emergency room

with a chief complaint of "feeling fatigued and having weight loss over a period of one month". Physical examination revealed the presence of an enlarged right testicle that the patient stated he had for the past 3 years. An ultrasound study was performed with the findings of a large heterogeneous echogenic mass with heterogeneous echotexture involving the right testicle measuring 13 x 12 x 9 cm in size.

Initial CT and MRI imaging showed a large right testis mass as well as extensive hepatic, retroperitoneal, pulmonary, and central nervous system (CNS) metastases with ventricular enlargement. Contrast CT of the abdomen and pelvis revealed a large 11 cm diameter heterogeneous mass arising from the right testicle with extension into right inguinal canal. Within the retroperitoneal tissues, there was a dominant large 6 x 3 cm low-density region suspicious for low-density lymphadenopathy. Within the liver, numerous confluent lesions formed a dominant mass measuring up to 10 x 18 cm. A mass effect of the right ureter was present causing mild right-sided hydronephrosis. Within the lung bases, there were several nodules compatible with metastatic disease measuring less than 2-3 cm in size each. A large lesion along the cardiac apex measuring 5 cm in size was also noted. The impression of these findings were consistent with metastatic malignancy.

Emergent ventricular shunt was placed in early February of 2012 followed by initiation of chemotherapy with Bleomycin, Etoposide and Cisplatin (BEP chemotherapy) along with a right radical orchiectomy. Pathological analysis was significant for Stage III Germ Cell Testicular Cancer, of the YST - type. Pre-treatment AFP level was elevated at 6933 ng/ml (normal: 0-5 ng/ml; Lab Corp®, Research Triangle Park, NC). CT of the head, chest, abdomen and pelvis repeated after 2 cycles early March 2012 revealed marked improvement in all metastatic lesions. By April 2012, the AFP levels decreased to 3.7 ng/ml. However, 4 months later, the disease progressed with increasing AFP (2441 ng/ml) along with CNS, systemic metastases in July 2012. Radiation therapy to the brain was then completed in early August 2012, and daily oral Etoposide was initiated. Significant progression in the size and number of pulmonary and hepatic metastases was noted in September 2012. Chemotherapy was resumed with Cisplatin, Ifosfamide (VIP chemotherapy) and Vinblastine in October 2012. VIP chemotherapy was completed after four cycles in December 2012. By February 2013, AFP levels began to rise again and the disease became very aggressive and metastasized further to the patient's lumbar and thoracic spine. He began Gemcitabine and Paclitaxel chemotherapy in February 2013. By June 2013 the AFP level was 13563 ng/ml. The patient died secondary to the extensive metastasis to his brain, spinal cord, liver, lung, and pelvis.

History was also notable for occasional consumption of alcohol. There is no known history of illicit drug use. The patient did smoke cigarettes since age 16-years; approximately 1-pack per day (i.e., 15-pack year history). Through secondary history, the patient was described as having an unhealthy diet. There were no known allergies. Until the time of death, neuropsychiatric health was unremarkable. The patient also fathered a daughter with autism spectrum disorder (ASD) born February, 2006.

RESULTS

Gross Examination and Dissection

Patient is a deceased, 31-year-old male that exhibited emaciated body habitus. He suffered from total body alopecia secondary to chemotherapy (a venous port was noted in the right, superior anterior thorax). The patient had a tattoo of a Chinese "symbol" on his left brachium and shoulder, and a second tattoo over the right pectoral region with his daughter's name. There was a scar over the right inguinal region status-post excision of right spermatic cord and right testis. There is significant and palpable hepatomegaly. Embalming incision is present over the right femoral triangle.

On dissection, the lungs appeared discolored with a non-homogeneous, black mottled pattern, likely due to long-standing tobacco use. Also noted were palpable lung masses bilaterally in the apex through the lung base. Numerous, small masses were adhered to the internal thoracic wall bilaterally. The heart and great vessels were normal. Extreme hepatomegaly was observed with the liver filling both left and right upper quadrants and extending down into the right lower quadrant adjacent to the right kidney, and multiple tumor masses were observed, some of which were adherent to the pancreas. Splenomegaly was observed, with the presence of tumors internally and on the splenic surface. Kidneys, ureters, urinary bladder and urethra were within normal limits. Metastatic tumors were observed on the thoracic (T12) and lumbar spine (L1 - L5), and the ala of the ilium bilaterally, the left-sided tumor penetrating through the bone. A shrunken tumor mass was observed in the central forebrain upon dissection. There were also a high-number of fascial adhesions throughout the patient's body.

Tissue Analysis

The specimen was received in formalin and was an inked, and consisted of an incised right testicle with an attached segment of spermatic cord. The testis weighed 356 g and had dimensions of 11.4 x 8.7 x 7.6 cm; and the spermatic cord had a length of 6.4 cm and a diameter that ranged from 1.6 cm proximally to 2.5 cm distally. The tunica was not freely mobile. The specimen was paraffin embedded, sectioned and processed with the standard

protocol for H&E.

Neoplastic mass entirely replaced testicular parenchyma; having invaded through the visceral tunica vaginalis and into the parietal tunica vaginalis. The mass entirely replaced the epididymis, rete testis and mediastinum testis, such that no normal testicular parachyma was identified. Parachyma was composed of primitive germ cells that form glomeruloid or embryonal-like structures, as well as areas with a micro-cystic histologic pattern and areas of fibrous dysplasia (Fig. 1A and 1B). Schiller-Duval body was also observed (Fig. 1C). The surface of the mass demonstrated hemorrhage and degeneration. The spermatic cord showed some induration with gray-yellow granularity and hemorrhage.

X-Ray Films

Post-mortem plain x-ray films were taken in the AP projection status-post 10 months since embalming. AP CXR (Fig. 2A) revealed a venous access port that can be seen on the right chest with catheter likely inserted into right subclavian vein and superior vena cava. The trachea was filled with air and was not deviated. The costodiaphragmatic recesses (or phrenicocostal sinuses) were seen bilaterally without blunting. Lung parenchyma was congested with blood vs. embalming fluid; lungs were underinflated. Opacities representative of lung masses were seen in the lung field bilaterally (Fig. 2A). The dome of the diaphragm over the liver and spleen was elevated; hepatomegaly was suggested (Fig 2A and Fig. 2B). Mild splenomegaly was observed. There was no evidence of osteoarthritis or degenerative disc disease; yet there appeared to be areas of non-homogeneity in the vertebral bodies as wells as the ribs.

AP Abdominopelvic film showed heterogeneous areas over the vertebral bodies, and several areas of radiolucency on the ala of the right ilium, and a larger area on the ala of the left ilium (Fig. 2B and 2C). There was a mixture of gas and feces in the colon. The liver extended inferiorly past R12. The small gut tube was filled with a mixture of flatus and solid material.

Left lateral lumbar spine film documented multiple areas of radiolucency in the vertebral bodies from T12 through L5, and compression fractures in
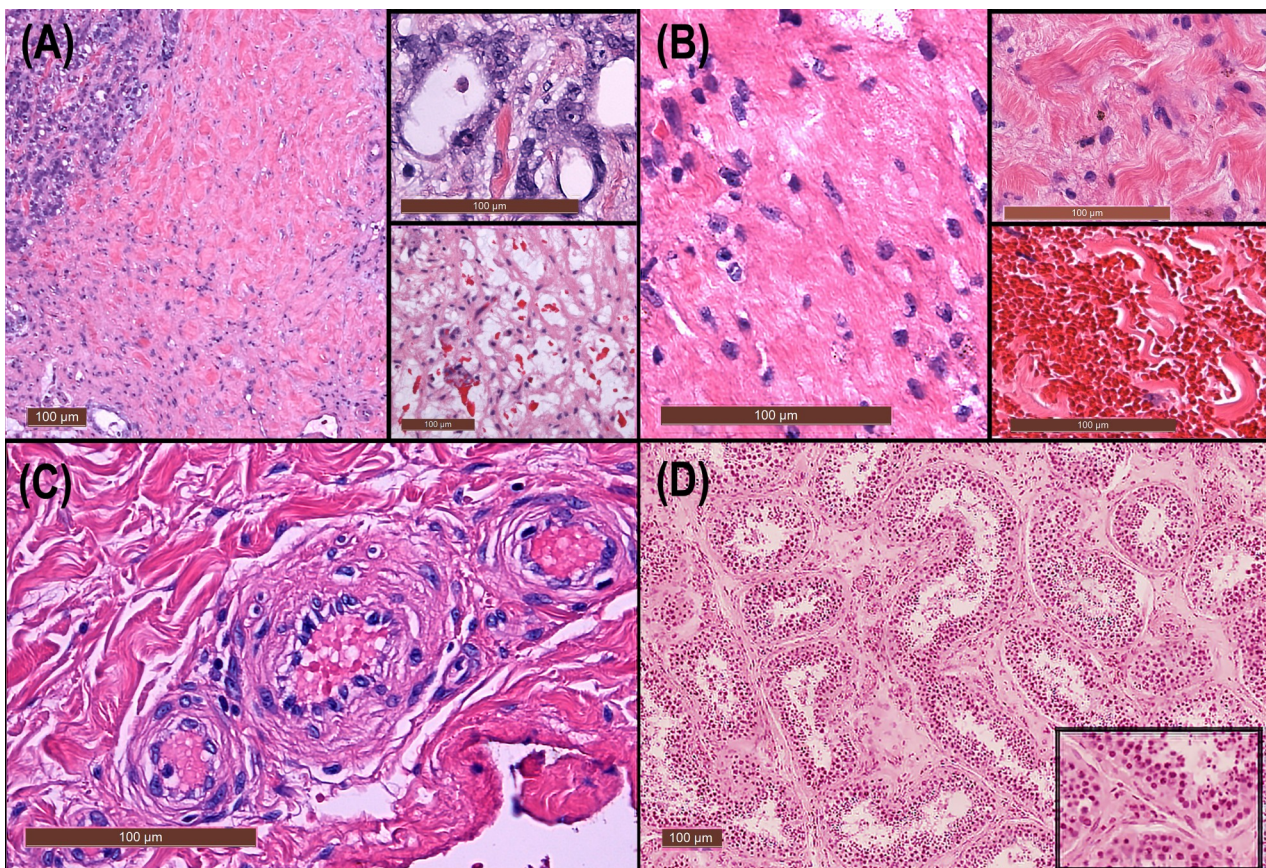

Fig 1. Histology of Testicular Tissue. **(A)** Survey view showing total lack of normal testicular parenchyma; with inset of glomeruloid (above) or embryonal-like structures and micro-cystic pattern (below). **(B)** Multiple areas of fibrous dysplasia without evidence of normal testicular parenchyma; with insets of higher-magnification fibrosis (above) and hemorrhage area (below). **(C)** Schiller-Duval bodies are distinctive perivascular structures seen in the endodermal sinus pattern of yolk sac tumor. Each consists of a central vessel surrounded by tumor cells – the whole structure being contained in a cystic space often lined by flattened tumor cells. It represents an attempt to form yolk sacs. **(D)** Section of normal testicular parenchyma with higher- magnification inset (lower right) (not provided by the patient described within this study).
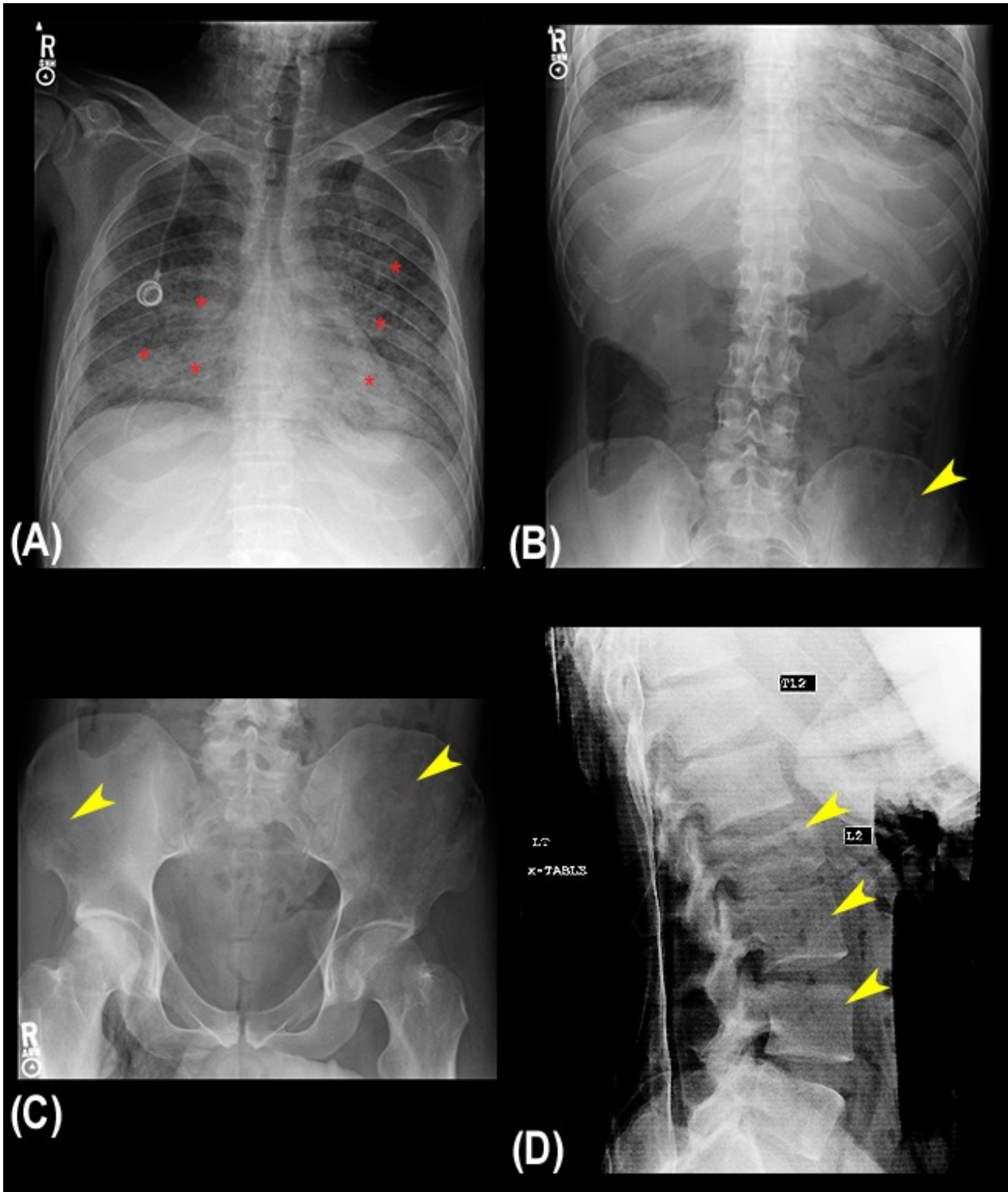
Fig 2. Plain X-Rays. Post-mortem, AP plain x-rays as shown. (A) AP CXR showing numerous opacities (red asterisk) in the L and R lung fields. The dome of the diaphragm over the liver is slightly elevated, and the liver and spleen are hyper-dense with hepato- and splenomegaly. (B) AP Abdominoplevic flat film demonstrating heterogenous area over the vertebral bodies, and several areas of radiolucency on the ala of the right and left (more prominent, yellow arrow) ilium. Hepatomegaly extends past R12. (C) AP Pelvis film clearly showing ala with increased radiolucency (yellow arrows). (D) Left Lateral view of lumbar spine showing multiple areas of hypo-density in vertebral bodies (yellow arrows) being most prominent at L2 (with compression fracture) and L3. There is also a compression fracture in T12. [Abbreviations: anterior-posterior (AP); chest x-ray (CXR); right (R); left (Lt); thoracic (T); lumbar (L)]

T12 and L2 (Fig. 2D).

Medical Imaging
  Surface Visualization. Ante-mortem films were used to construct a surface 3-D visualization of the patient's pelvic area, enlarged scrotum and testicular mass (see Table 1 and Video Clip 1.).
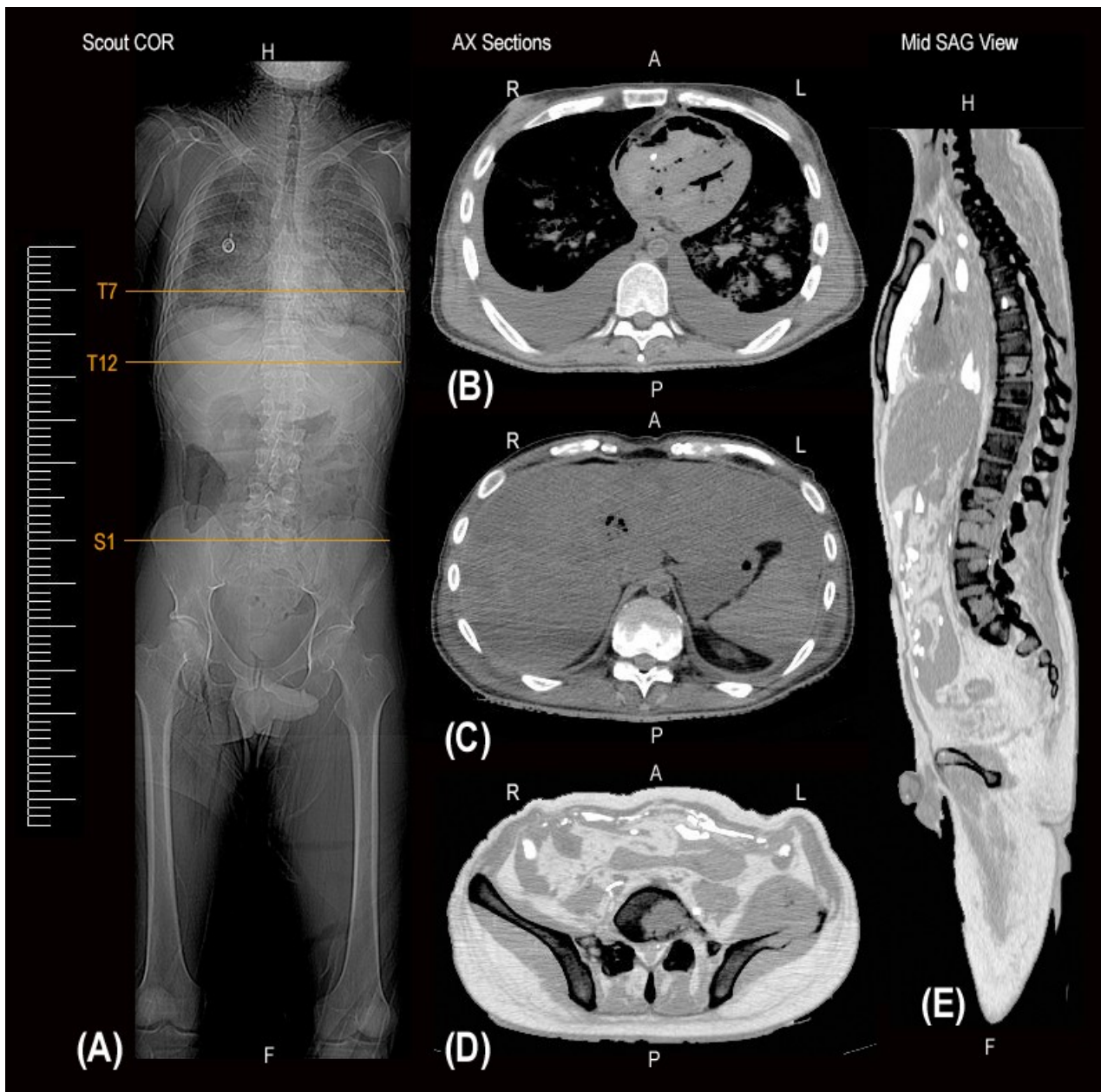
Fig 3. Computed Tomography. (A) COR Scout View of patient showing multiple densities in the thorax; increased density of the hepatic and splenic areas and radiolucency in the ala of the left ilium. (B) AX CT of Thorax at vertebral level T7 (see "A") showing multiple metastatic foci in the L and R lung fields. (C) AX CT of Abdomen at vertebral level T12 (see "A") showing extensive hepatomegaly the multiple tumors and invasion of tumor into vertebral body. (D) Contrast inverted AX CT of superior pelvic region at vertebral level S1 showing metastatic infiltration into S1 and through the L ilium. (E) Contrast inverted mid-SAG CT showing tumor infiltration vertebral bodies at multiple levels. [Abbreviations: Anterior (A), Axial (AX), Computed Tomography (CT), Coronal (COR), Foot (F), Head (H), Left (L), Posterior (P), Right (R), Sacral (S), Sagittal (SAG), Thoracic (T).]

CT Scan. Post-mortem scout views (Fig. 3A), series and recon-sequences were carefully reviewed, and sequences taken in AX view were reformatted using MPR to SAG and COR series. These series, as well as their inverted counterparts, were evaluated. Head CT showed calcification of the choroid plexus at midline and bilaterally inside the ventricular atrium (i.e., calcified glomus). Calcification was normal, non-pathological finding. Multiple tumor masses were observed within the lung parenchyma (Fig. 3A and 3B): 5 cm, 4 cm, 3 cm and 2.1 cm in the inferior left, posterior lobe; 9 cm and 1.0 cm in the anterior lobe, and 3 cm and 2 cm in the right lower lobe. Some tumor invasion was observed in the ribs bilaterally. Extensive hepatomegaly (Fig. 3A and 3C) was present; extending over to the contralateral mid-clavicular line and unilaterally past R12. The liver contained multiple masses of varying sizes and these were scattered throughout the liver parenchyma at all levels. The gallbladder was present and did not contain sludge or gallstones. A large 7.4 x 9.7 cm mass (Fig. 3A and

247

Table 1. Summary of Features in Reconstructions and Video Clips.

BodyViz® Video Clip	Summary of Features
Video Clip 1. Surface 3D-Visualization and Testicular Mass	Surface views of enlarged scrotum with right testicular mass Axial dissection Oblique dissection highlighting irregular tumor mass in right testicle
Video Clip 2. Radiographic Brain Dissection with Ventricular Fly-Through	Axial dissection of head showing enlarged ventricles and large central tumor mass Coronal dissection documenting tumor mass in center of ventricular cavity penetrating septum pellucidum Sagittal dissection with lateral view of tumor mass Tumor mass (mid-sagittal): measurement = 38.45 mm Tumor dissection: digital subtraction on non-tumor (cancerous) tissue (i.e., isolation of tumor mass) Isolated overlay of tumor with ventricles; 360° rotational view Ventricular Fly-Through with highlighted tumor
Video Clip 3. Radiographic Dissection of Liver Metastases	Axial dissection of liver Axial dissection of liver with extreme hepatomegaly; enhanced tumor masses and overlays (superior view)
Video Clip 4. Radiographic 3D-Visualization: Thorax and Tumors	Axial dissection of thorax; reconstruction with multiple tumor masses Coronal dissection showing multiple tumor masses Axial dissection with measurement of tumor masses: 40.72 mm; 45.85 mm; 36.67 mm, 32.57 mm, 10.67 mm, 10.49 mm, 15.41 mm (**left lung**); 31.90 mm; 28.99 mm, 6.37 mm; 7.84 mm, 76.11 mm, 67.42 mm, 4.69 mm, 8.94 mm ,5.66 mm, 9.32 mm, 10.83 mm, 10 mm and 3.26 mm (**right lung**)
Video Clip 5. Radiographic 3D-Visualizaton; Pelvic Infiltration of Testicular Cancer	Axial dissection Coronal dissection Bony pelvis reconstruction with highlighted area of penetrating tumor mass; 360° rotational view
Video Clip 6. Radiographic Dissection and 3D- Visualization: Spine Metastases	Axial dissection of vertebral column Sagittal dissection of thoraco-lumbar spine with multiple tumors (T12 - S1) and impingement on spinal cord (L2 and L3) – highlighted overlays Axial dissection with highlighted overlays of tumors within vertebral bodies; also showing impingement on spinal cord.

3D) in the left iliac fossa was observed to be infiltrating through the bone and into the gluteal muscle. There were multiple tumor metastases throughout the lumbar and thoracic spine (Fig. 3E) as well as the sacrum, and up to C7. In the lumbar region, tumors compress the spinal cord in the anterior spinal canal (Fig. 3E).

MRI Scan. Frames in all series were evaluated using MPR in AX, COR and SAG views and T1-T2 weighting; and AX T2 FLAIR; FRFSE T2 and FRF-SE T2 2 NEX, T2 GRE and AX T2 FLAIR were used for brain scans. A central ventricular tumor mass was present and measured 44 mm x 35 mm and 1169.52 mm2 (area) (Fig. 4A and 4B; see Table 1 and Video Clip 2.). There was bilateral enlargement of the lateral ventricular system, or obstructive hydrocephalus. Tumor mass and ventricular enlargement resulted in an 8 mm shift of mid-brain structures of the right of midline. There were additional amorphous masses of tissues in the right lateral ventricle and the medial parietal lobe (with fluid). There were multiple masses that measured approximately 4.4 x 2.1 cm in the apex of the left lung, and masses that measured 2.5 cm - 4 cm in diameter in the lower right lobe (slices not shown; see Table 1 and Video Clip 4.). Hepatomegaly (Fig. 4C) was demonstrated reaching to the contralateral thoracic cage: 24.1 x 13.9 cm. Numerous tumor metastases were present ranging from 6 mm to 4.7 cm in diameter (see Table 1 and Video Clip 3.). Gallbladder was present. There was a mixture of fecal matter and flatus in the large intestine, as well as contents throughout the small bowel. The stomach was filled with gas and chyme, and rugae were visible. A large tumor was observed in the left pelvis and extending through the ilium into the gluteus minimus and medius muscles (MRI not shown; see Table 1 and Video Clip 5.; CT Scan – Fig. 3). Multiple metastases were noted throughout the sacrum, and lumbar and thoracic regions of the vertebral column (MRI not shown here, see Table 1 and Video Clip 6.; CT Scan – Fig. 3).

High-Resolution Image-Reconstruction and Video Clips

BodyViz® was used to reconstruct DICOM files into video clips for 3-D image analysis. The results are summarized in Table 1 and video clips can be view by opening the hyperlinks.

DISCUSSION

Testicular cancers are not a common malignancy in the United States or internationally; however, the incidence rate has been increasing in the U.S. and many other countries for several decades. It is estimated that about 8,850 new cases of TC will be diagnosed in the year 2017 in the United States

with around 410 deaths from TC. Of these, 50% occur in males ranging from 20-34 years old and most commonly in white males (American Cancer Society, 2017; Trabert et al., 2015; Ghazerian et al., 2015). This is significant because the patient discussed here fits these criteria. What is *uncommon* in this case is the *type* of tumor. YST, or endodermal sinus tumor, is a type of Nonseminoma. Testicular Germ Cell Tumor originates in cells that line the yolk sac of the embryo. Early in embryogenesis, these cells migrate into the developing gonadal ridge (or genital ridge) that is the precursor to the gonads (i.e., the ovaries in females, and the testes in males). Occurring most frequently in children, it can also present in young adults. In the latter case, this tumor is often found mixed with other types of tumor, in particular, teratoma and embryonal carcinoma-types (Talerman, 1980; Sesterhenn and Davis, 2004). Histological studies in this case demonstrate that this patient had a *pure* form of YST with glomerular and microcytic patterns and fibrosis; without any other TC tumor types (see Fig. 1 A-D). The prognosis is favorable in children, but in young adults, the tumor becomes aggressive and tends to metastasize rapidly making the prognosis poor, and even worse in the case of brain metastasis (Feldman et al., 2016; Leman and Gonzalgo, 2010).

The etiology of YSTs is essentially unknown. It is speculated that hypermethylation of the *RUNX3* gene promoter and overexpression of GATA-4, a transcription factor that regulates differentiation and function of yolk sac endoderm, may play important roles in the pathogenesis of YSTs (Kato et al., 2003; Siltanen et al., 1999). However, these hypotheses have not been confirmed. Other studies have identified several genetic loci that confer a predisposition to TC with the most common being detected at 12q21 (Adra and Einhorn, 2017). Most TC cells have extra copies of a part of chromosome 12 called isochromosome 12p (Adra and Einhorn, 2017; American Cancer Society, 2016).

Risk factors for TC are not well characterized. However, a strong relationship between cryptorchidism and TC has been identified. Other factors associated with TC include a prior unilateral TC, race and family history (McGlynn and Trabert, 2012). What we do know about Josh was that his diet was unhealthy and he was a 15 pack-year smoker, yet these aspects of his social history have no proven correlation to TC. He had no family history of TC and did not have cryptorchidism.

Staging of Testicular Cancer

Staging of testicular tumors includes determination of the tumor (T), node (N), metastasis (M) and serum tumor markers (S) categories. Requirements for the clinical staging include clinical examination and histological assessment as well as radiographic assessment of the chest, abdomen and pelvis. Serum tumor markers included in this stag-

ing process include AFP, hCG, and LDH, which are obtained prior to orchiectomy. With regard to pathological staging, histological evaluation of the radical orchiectomy specimen must be used for the pT classification (i.e., primary tumor classification; AJCC Cancer Staging Mannual, 2010).

The patient's pathological staging at the time of diagnosis/orchiectomy was pT1 pNX pM1b S2. By definition, the patient's tumor was assessed as being limited to the testis and epididymis without vascular/lymphatic invasion; tumor may invade into the tunica albuginea but not the tunica vaginalis. For the node portion of the staging, NX represents that his regional lymph nodes could not be assessed. Metastatic staging for this patient was defined as M1b, which represented distant metastases other than to non-regional lymph nodes and lung. Therefore, at the time of diagnosis, Stage IIIC was the anatomic stage/prognostic group to which the patient was assigned (AJCC Cancer Staging Manual, 2010).

Metastatic Patterns of Testicular Cancer

For both seminoma and nonseminoma TC, metastasis occurs primarily to the retroperitoneal lymph nodes and subsequently further along the thoracic duct. Spreading can also occur hematogenously, especially for nonseminomas. About 20% of patients having seminoma tumors have metastases at the time of diagnosis, most often lymph node metastases to the retroperitoneum and/or the supraclavicular region (Hu et al., 2015; Woldu and McKieman, 2015; Karesen and Wist, 2005). Nonseminomas often display rapid spreading, and about 50% of patients have metastases at the time of diagnosis (Karesen and Wist, 2005; Stevenson and Lowrance, 2015).

Fizazi et al. (2001) described the distribution of extra-retroperitonal masses resected in patients who relapsed following Cisplatin therapy. The lung (52%) was most commonly involved, followed by the mediastinum (28%), cervical nodes (7%), liver (4%), bone (1.6%) and brain (0.8%). Masterson et al. (2012) reviewed the sites of disease in 130 patients and found a similar distribution (lung in 68%, mediastinum 29%, liver 13%, neck 12%). Thus, when diagnosing, evaluating and treating patients with metastatic TGCT, an understanding of the patterns of disease is required.

Lymphatic Spread. Lymphatic drainage from the retroperitoneum (RP) plays a major role in determining the pattern of dissemination (Hu and Daneshmand, 2015; Woldu and McKieman, 2015). Lymphatic vessels draining the testis course in a retrograde fashion in a plexus along the testicular artery. This is in contrast to the drainage of the scrotum, where vessels course adjacent to the cremasteric artery; then empty into superficial inguinal lymph nodes. Proximal to the abdominal aorta at approximately level L2-L3, vessels enter lumbar (caval/aortic) lymph nodes and then travel to pre-

aortic lymph nodes that empty into the cisterna chyli. Some lymph vessels traveling along the testicular artery empty directly into the cisterna chyli. The cisterna chyli gives rise to the thoracic duct (at about T12) that traverses the diaphragm at the aortic aperture and ascends the superior and posterior mediastinum between the descending thoracic aorta (to its left) and the azygos vein (to its right). Near the root of the neck, it curves posteriorly to the left carotid artery and left internal jugular vein at the T5 vertebral level. It drains into the systemic (blood) circulation at the angle of the left subclavian and internal jugular veins as a single trunk, at the commencement of the brachiocephalic vein, below the clavicle, near the shoulders. From this point, TC may have spread throughout the body.

Because para-aortic and paracaval lymph nodes drain behind the crura of the diaphragm to the middle mediastinum, the middle mediastinum is the *most common* mediastinal compartment involved in TGCT, and can be divided into 3 regions: (1) superior (thoracic inlet to carina); (2) mid (carina to dome of the diaphragm); (3) inferior (dome of diaphragm to diaphragmatic crura). Spread to the anterior and posterior compartment likely occurs secondary to lymphatic obstruction and retrograde flow. Kesler (2002) confirmed this hypothesis in a study that reviewed 268 patients with metastatic mediastinal TGCT, in whom the anterior and posterior compartments were only involved if concurrent with middle mediastinal disease. Of the patients examined, metastatic TGCTs were identified in the anterior compartment (7%); posterior compartment (14%), and the middle mediastinum (157%: superior (44%), mid (67%) and inferior (46%)).

Clinical significance is related to malignancy, where the first sign of a malignancy, especially an intraabdominal one, may be an enlarged Virchow's node. A Virchow's node is a lymph node in the left supraclavicular area, in the vicinity where the thoracic duct empties into the left brachiocephalic vein, between where the left subclavian vein and left internal jugular join (i.e. the left Pirogoff angle). Further, when the thoracic duct is blocked or damaged, a large amount of lymph can quickly accumulate in the pleural cavity (i.e., known as chylothorax). Thus, the Virchow's node is considered to be a sentinel lymph node, or the hypothetical first lymph node or group of nodes draining a cancer. In case of established cancerous dissemination, it is postulated that the sentinel lymph node is the first node reached by metastasizing cancer cells from the tumor.

The concept of the sentinel lymph node is important because of the advent of the sentinel lymph node biopsy technique, also known as a sentinel node procedure. This technique is used in the staging of certain types of cancer to see if they have spread to any lymph nodes, since lymph node metastasis is one of the most important prognostic signs. It can also categorize the TC to be inter-aortocaval, paracaval or common iliac region in patients with right-sided TC, as in the patient discussed herein, versus para-aortic lymph nodes in patients with left-sided cancer (Hu and Daneshmand, 2015; Ohyama et al., 2002; Brouwer et al., 2011; Kesler, 2002).

Hematogenous Spread. *Arterial.* The primary arterial supply to the testis are the paired testicular arteries that arise from the abdominal aorta at level L2. These arteries descend through the inguinal canal as a component of the spermatic cord. In contrast, the internal pudendal artery (a branch of the internal iliac artery) supplies the scrotum and the rest of the external genitals. The testis also has collateral blood supply from (1) the cremasteric artery (a branch of the inferior epigastric artery – which is a branch of the external iliac artery), and (2) the artery to the ductus deferens (a branch of the inferior vesical artery – which is a branch of the internal iliac artery). If TGCT cells escape the microvasculature (i.e., capillary bed), then they may enter lymphatic vessels surrounding the testicular artery (i.e., the primary lymphatic route), or those lymph vessels adjacent to the cremasteric artery or the artery to the ductus deferens. Cancerous cells that escape microvasculature, may also invade surrounding tissue via direct infiltration. Even further, TGCT are often vascular (or hypervascular) (Silvan, et al., et al. 2015); thus, increasing the potential for hematogenous spread. Epididymo-orchitis may be idiopathic or may be the result of viral (i.e., mumps) or bacterial infection, or associated with TC (Gupta et al., 2014). If present, or if present alone (i.e., epididymitis or orchitis), retrograde (or reversal) of diastolic arterial blood flow can result (Marks et al., 2009), and this may lead to retrograde metastasis of TGCTs secondary to "dumping" of metastatic TGCT cells/foci at the aortic orifice of the testicular artery or the common iliac artery. Still further, retrograde flow along the route leading to the common iliac artery, might also result in escape of TGCT cells/foci into the tissue space adjacent to soft tissues of the anterior iliac fossa. This may be one possible origin for the large tumor penetrating the ala of the left ilium in this patient (Fig. 3D; Table 1 and Video Clip 5.).

With particular reference to the metastases of the thoracic and lumbar spine of the patient in the case discussed here, periosteal and equatorial branches of cervical and segmental arteries and their spinal branches supply the vertebrae of the spinal column. These vessels occur at all levels of the vertebral column and include vertebral and ascending cervical arteries (neck), and major segmental arteries of the truck: posterior intercostal arteries (thorax); subcostal and lumbar arteries (abdomen); and iliolumbar and lateral sacral arteries (pelvis).

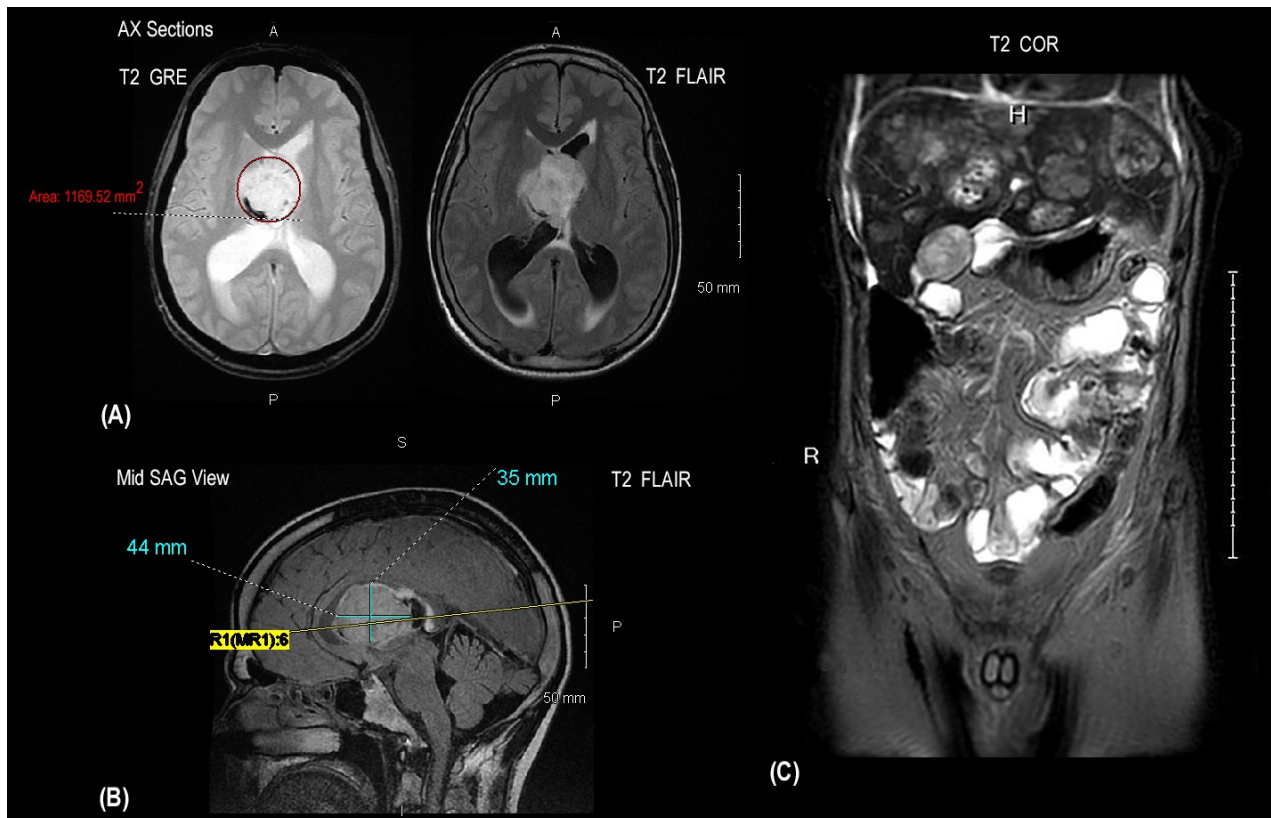Periosteal and equatorial arteries arise from ar-

Fig 4. Magnetic Resonance Imaging. (A) T2-weighted AX images of the brain without (GRE) and with (FLAIR) suppression of signal from cerebrospinal fluid showing centralized tumor focus with area of 1169.52 mm2 and obstructive hydrocephalus of the lateral ventricles. (B) T2-weighted Mid SAG view showing tumor with dimensions of 44 x 35 mm. (C) T2-weighted COR abdominopelvic view with extensive hepatomegaly and liver parenchyma filled with multiple tumors of various sizes.

teries (above) as they cross the anterolateral surface of the vertebrae. Then, spinal branches enter the intervertebral (IV) foramina and divide into small anterior and posterior vertebral canal branches pass to the centrum and vertebral arch. These vessels, in turn give rise to ascending and descending branches that anastomose with branches from adjacent levels. The anterior vertebral canal branches also give rise to nutrient arteries that supply the body/marrow. Larger branches of spinal arteries continue as terminal radicular or segmental medullary arteries to the anterior and posterior roots and meninges. Once at the meninges, metastases can spread to the brain (Fig. 4 A and B; Table 1 and Video Clip 2.) by this route, or via entry into (and subsequent circulation of) cerebrospinal fluid.

Venous. The pattern of venous drainage of the testes reflects paired veins, with one receiving blood from each testis. The right testicular vein generally joins the inferior vena cava (IVC); the left testicular vein, unlike the right one, joins the left renal vein, which then drains into the IVC. Veins emerge from the back of the testis, and receive tributaries from the epididymis; they unite and form a convoluted plexus, called the pampiniform plexus, which constitutes the greater mass of the spermatic cord; the vessels composing this plexus are very numerous, and ascend along the cord, in front of the ductus deferens.

Below the subcutaneous inguinal ring, they unite to form three or four veins, which pass along the inguinal canal, and, entering the abdomen through the abdominal inguinal ring, coalesce to form two veins, which ascend on the Psoas major, behind the peritoneum, lying one on either side of the internal spermatic artery. These unite to form a single vein, which opens, on the right side, into the IVC (at an acute angle), on the left side into the left renal vein (at a right angle). In the present case, the former route was likely taken secondary to right-sided TGCT, and as supported by histologic evidence of invasion along the right spermatic cord. Once inside the IVC, cancerous cells may spread to the lungs, mediastinum, liver and spleen (via the celiac trunk), brain (via the internal carotid or vertebral arteries) and throughout the entire body.

Spinal veins form plexuses along the vertebral column (inside-and-outside of the spinal canal). The internal vertebral venous plexus (i.e., epidural venous plexus) can be divided into the anterior and posterior internal vertebral plexuses, coursing along the anterior and posterior portions of the spinal canal, respectively. The external vertebral venous plexus is also divided into anterior and posterior components on the respective external surfac-

es of the vertebrae. Plexuses communicate via IV foramina - more dense anteriorly and posteriorly (sparse laterally); which may correlated to increased tumor density in the centrum of vertebrae as compared to posterior arch components in this patient's spinal column lesions. The basivertebral vein is a large, tortuous vein that forms within vertebral bodies and drains into the anterior external and internal plexuses at its anterior margin. Intervertebral veins receive veins from the spinal cord, as well as the vertebral venous plexuses, and drain into veins of the neck and segmental (intercostal, lumbar and sacral) veins of the trunk. All of these anastomoses can contribute to metastasis of TGCT either (1) after infiltration of tumor cells from established metastatic foci in the centrum secondary to arterial spread; or (2) through direct hematogenous spread via venous plexuses and then larger veins.

Direct Tissue Invasion (or Infiltration). Once the tumor cell has arrived at a likely point of intravasation, it interacts with the endothelial cells by undergoing biochemical interactions (mediated by carbohydrate-carbohydrate locking reactions, which occur weakly but quickly). These biochemical reactions enable the tumor cell to develop adhesions to endothelial cells to which the tumor cell forms stronger bonds, and thus the tumor cell penetrates the endothelium and the basement membrane (Ono et al., 1999; Martin et al., 2013). This process is termed extravasation The new tumor can then proliferate at this secondary focus. The metastatic cascade is therefore dependent on the loss of adhesion between cells, which results in the dissociation of the cell from the primary tumor, and subsequently the ability of the cell to attain a motile phenotype via changes in cell to matrix interaction.

Several molecules have been identified as having important roles to play in the signaling processes leading to cell motility/migration, with the associated loss of epithelial characteristics and gain of a migratory and mesenchymal phenotype (i.e., Epithelial-Mesenchymal Transition, or EMT). Thus, the acquisition of a mesenchymal-like cell phenotype provides one of the major characteristics of metastatic progression of most carcinomas. Loss of expression of the cell-cell adhesion molecule E-cadherin is a characteristic trait of EMT in development and in the progression of epithelial tumors to invasive, metastatic cancers. The loss of E-cadherin is generally seen to coincide with a gain of expression of the mesenchymal cadherin, N-cadherin in many cancer types; this 'cadherin switch' is thought to be necessary for tumor cells to gain invasive properties and is also a characteristic of EMT (Cavallaro and Christofori, 2014).

It is evident from recent studies that EMT-inducing signals are, in part, initiated by growth factors, including hepatocyte growth factor (HGF), epidermal growth factor (EGF) and transforming growth factor β (TGFβ). These induce downstream activation of a number of EMT-inducing transcription factors including Snail, Slug, Twist and zinc finger E-box binding homeobox 1 (ZEB1) (Thiery, 2002; Cano et al., 2000; Peinado et al., 2007; Medici et al., 2008).

The growth of new blood or lymphatic vessels from pre-existing vessels (the process of angiogenesis or lymphangiogenesis) is essential in physiological events such as reproduction, development, wound-healing and immunity. However, imbalance or manipulation of these essential processes *facilities tumor growth and direct infiltration* involved in cancer progression and metastasis (Folkman, 2007; Potente et al., 2011).

The angiogenic process is made up of a complex multi-step cascade, which is tightly regulated through the balance of a number of pro- and anti-angiogenic factors. Tumor cells frequently tip this balance in favor of blood vessel production through the secretion of pro-angiogenic factors (Martin, 2013). The production of angiogenic factors from a tissue or tumor bind to and activate endothelial cells of a neighboring blood vessel. Following activation, the endothelial cells begin to produce enzymes that break down the basement membrane of the blood vessel creating tiny pores. Endothelial cells then proliferate and migrate through these pores, toward the angiogenic source. This migratory mechanism involves a variety of adhesion molecules to aid movement of the new blood vessel toward the source and also the production of various enzymes, such as matrix metalloproteinases, at the sprouting tip, to facilitate this movement through the extra- cellular matrix (Martin, et al., 2013). Endothelial cells of the new vessel then undergo a tubule formation phase, forming a tube-like structure before establishment of a blood vessel loop between the source and the existing vessel. This vessel loop is stabilized through recruitment of additional cell types, such as smooth muscle cells, providing support to the vessel and allowing blood flow to the angiogenic source (Pandya et al., 2006).

Metastasis, the leading cause of mortality in patients with cancer, is receiving increasing attention in both scientific and clinical research. Yet, the mechanisms remain poorly understood, and methods in combatting metastasis remain limited. However, with the increasing knowledge in gene expression, cellular behavior, biological events in the spread paths of cancer cells, there are now new prospects of taking some of the observations into the diagnosis, prognosis and treatment in the metastatic disease. Although enormous challenges remain, these lines of basic science research will lead to clinical practice.

CONCLUSION

This investigation has described a case of stage III TGCT of yolk-sac type in an adult male with metastases to nodes, bone, viscera and brain. *This*

case is interesting because (1) it differs from the usual TC type found in adult (vs. young) males; (2) it presents a histological tumor-type consistent with a pure form of YST with both glomerular and microcytic patterns and fibrosis; (3) it reveals the presence of a large intraventricular brain tumor, and (4) multiple routes of metastatic disease. TC is the most common diagnosed cancer in young men. Although there are multiple risk factors of the disease, cryptorchidism, infertility, and others, most cases represent sporadic occurrences. Most commonly, this disease presents as an early stage (clinical stage 1) and is highly curable with radical orchiectomy, in contrast to the most critical scenario with brain metastases. The embryonic origin of the testis in the RP and, therefore, lymphatic drainage pattern informs the most common location of metastatic disease. Thus, successful management of TGCTs has been facilitated by a predictable pattern of metastatic spread of disease, primarily to the lymph nodes of the RP and subsequently to the lung and posterior mediastinum. Given the patterns of metastatic spread (i.e., left vs. right TC), RPLND has a well-established role in the management of disease. Even further, surgery has a critical role in treating metastatic TGCT outside of the RP. Secondary to the worldwide increasing incidence of TC, and because surgeries can be safely combined with adjuvant therapies but have potential for significant morbidity, a multidisciplinary team with *expert* knowledge of *anatomical patterns* of metastasis and experience in treating TGCT is essential for optimal patient outcomes.

VIDEO CLIPS

Video Clip 1. Surface 3D-Visualization and Testicular Mass

Video Clip 2. Radiographic Brain Dissection with Ventricular Fly-Through

Video Clip 3. Radiographic Dissection of Liver Metastases

Video Clip 4. Radiographic 3D-Visualization: Thorax and Tumors

Video Clip 5. Radiographic 3D-Visualizaton; Pelvic Infiltration of Testicular Cancer

Video Clip 6. Radiographic Dissection and 3D-Visualization: Spine Metastases

EDUCATION NOTE

This research study has been presented as a clinical anatomy workshop in the Continuing Medical Education, Grand Round Series at Union Hospital and at its affiliates (Terre Haute, IN), as well as in the formats of research seminar and anatomy education/review didactic presentations in the Department of Biological Sciences at Indiana University Northwest (Gary, IN) and the Department of Anatomy & Cell Biology at the Indiana University School of Medicine. All post-program evaluation surveys from clinicians, anatomists, and students, have been overwhelmingly positive with the "information presented found to be useful in research, education and clinical practice", and clinicians stated, "The information herein has changed the way that I will approach possible TC in their patients."

NOTES ON CONTIBUTORS

ERNEST F. TALARICO, JR., Ph.D., is Associate Professor of Anatomy & Cell Biology and Site Director for Human Structure at the Indiana University School of Medicine-Northwest (Gary, IN), and is Step Master for Human Structure, and Course Director of Human Gross Anatomy, Embryology & Radiology. Dr. Talarico holds a joint appointment as Associate Faculty in the Department of Radiologic Sciences at Indiana University Northwest. He created and serves as director for the International Human Cadaver Prosection Program, which in 2008 received the award for most outstanding and innovative program in undergraduate and continuing medical education from the AAMC Central Group on Educational Affairs. He is creator of the "Talarico Protocol for Human Gross Anatomy" and is the 2008 recipient of the Partnership Matters Award from the Northwest Indiana Area Health Education Center. In recognition of his work and innovations in anatomical education, in October 2010, Dr. Talarico was inducted as a fellow into the Northwest Indiana Society of Innovators. Currently, Dr. Talarico also serves as the director of the Anatomy Project in Vietnam and Southeast Asia.

JOSE L. MAS, D.V.M., is a graduated with a Doctor of Veterinary Medicine from National University of the Northeast (Corrientes, Argentina), where he served as professor of Anatomy (Anatomy II) in the School of Veterinary Medicine.

Dr. Mas was an Assistant Professor of Anatomy and Physiology and Advance Human Physiology at Ivy Tech College (Gary, Indiana). For the past 2-years, he has served in the position of Assistant Clinical Professor of Human Anatomy and Cell Biology at the Indiana University School of Medicine - Northwest (Gary, Indiana). Since 2011, he has also been a team leader and instructor for the International Human Cadaver Prosection Program.

JONATHAN A. JONES, M.D., M.P.H., is a former Postdoctoral Fellow at the Indiana University School of Medicine - Northwest (Gary, IN), where he worked extensively with the Human Anatomy department and in the International Human Cadaver Prosection Program. Dr. Jones earned his Master's in Public Health at St. George's University School of Medicine (Grenada, West Indies) and then went on to earn his medical degree, where he graduated Summa Cum Laude, from American University of Antigua School of Medicine (Antigua, West Indies). He is currently a Family Medicine Resident at Union Hospital (Terre Haute, Indiana).

REFERENCES

ADRA N, EINHORN LH (2017) Testicular cancer update. *Clin Adv Hematol Onco*, 15(5): 386-396.

AMERICAN CANCER SOCIETY (2016) Do we know what causes testicular cancer? Available at: https://www.cancer.org/cancer/testicular-cancer/causes-risks-prevention/what-causes.html

AMERICAN CANCER SOCIETY (2017) What are the key statistics about testicular cancer? Available at: https://www.cancer.org/cancer/testicular-cancer/about/key-statistics.html

BEARD CJ, GUPTA S, MOTZER RJ, O'DONNELL EK, PLIMACK ER, MARGOLIN KA, RYAN CJ, SHEINFELD J, FELDMAN DR (2015) Follow-up management of patients with testicular cancer: A multidisciplinary consensus-based approach. *JNCCN Journal of the National Comprehensive Cancer Network*, 13(6): 811-822.

BEYER J, ALBERS P, ALTENA R, APARICIO J, BOKEMEYER C, BUSCH J, CATHOMAS R, CAVAL-LIN-STAHL E, CLARKE NW, DAHL AA, DAUGARRD G, et al. (2013) Maintaining success, reducing treatment burden, focusing on survivorship: highlights from the third European consensus conference on diagnosis and treatment of germ-cell cancer. *Ann Oncol*, 24 (4): 878-888.

BOYLE HJ, JOUANNEAU B, DROZ JP, FLECHON A (2013) Management of brain metastases from germ cell tumors: a single center experience. *Oncology*, 85 (1): 21-16.

BROUWER OR, VALDES OLMOS RA, VERMEEREN L, HOEFNAGEL CA, NIEWEG OE, HORENBLAS S (2011) SPECT/CT and a portable gamma-camera for image-guided laparoscopic sentinel node biopsy in testicular cancer. *J Nucl Med*, 52(4): 551-554.

CANO A, PEREZ-MORENO MA, RODRIGO I, LOCAS-CIO A, BLANCO MJ, DEL BARRIO MG, PORTILLO F,

NIETO MA (2000) The transcription factor snail controls epithelial-mesenchymal transitions by repressing E-cadherin expression. *Nat Cell Biol*, 2(2): 76-83.

CAVALLARO U, CHRISTOFORI G (2004) Cell adhesion and signalling by cadherins and Ig-CAMs in cancer. *Nat Rev Cancer*, 4(2): 118-132.

CHIA VM, QURAISHI SM, DEVESA SS, PURDUE MP, COOK MB, MCGLYNN KA (2010) International trends in the incidence of testicular cancer, 1973-2002. *Cancer Epidemiol Biomarkers Prev*, 19(4): 1151-1159.

CHOUEIRI TK, STEPHENSON AJ, GILLIGAN T, KLEIN EA (2007) Management of clinical stage I nonseminomatous germ cell testicular cancer. *Urol Clin North Am*, 34(2): 137-148.

COOK MB, AKRE O, FORMAN D, MADIGAN MP, RICHIADI L MCGLYNN KA (2009) A systematic review and meta-analysis of perinatal variables in relation to the risk of testicular cancer– experiences of the mother. *Int J Epidemiol*, 38(6): 1532-1542.

COOK MB, OLOF A, FORMAN D, MADIGAN MP, RICHIARDI L, MCGLYNN KA (2010) A systematic review and meta-analysis of perinatal variables in relation to the risk of testicular cancer— experiences of the son. *Int J Epidemiol*, 39(6): 1605-1618.

ELZINGA-TINKE JE, DOHLE GR, LOOIJENGA LHJ (2015) Etiology and early pathogenesis of malignant testicular germ cell tumors: towards possibilities for preinvasive diagnosis. *Asian J Androl*, 17(3): 381-393.

FELDMAN DR, LORCH A, KRAMAR A, ALBANY C, EINHORN LH, GIANNATEMPO P, NECCHI A, FLECHON A, BOYLE H, CHUNG P, HUDDART RA, BOEKMEYER C, TRYAKIN A, SAVA T, WINQJUIST EW, DE GIORGI U, APARICIO J, SWEENEY CJ, CHON CEADERMARK G, BEYER J, POWLES T (2016) Brain metastases in patients with germ cell tumors: prognostic factors and treatment options – an analysis from the global germ cell cancer group. *J Clin Oncol*, 34(4): 345-351.

FERGUSON L, AGOULNIK AI (2013) Testicular cancer and cryptorchidism. *Front Endocrinol (Lausanne)*, 4 (32): 1-9.

FERLAY J, STCLIAROVA-FOUCHER E, LORTET-TICULENT J, ROSSO S, COEBERGH JWW, COMBER H, FORMAN D, BRAY F (2013) Cancer incidence and mortality patterns in Europe: Estimates for 40 countries in 2012. *Eur J Cancer*, 49(6): 1374-1403.

FIZAZI K, TJULANDIN S, SALVIONI R, GERMA-LLUCH JR, BOUZY J, RAGEN D, BOKEMEYER C, GERL A, FLECHON A, DE BONO JS, STENNING S, HORWICH A, PONT J, ALBERS P, DE GIORGI U, BOWER M (2001) Viable malignant cells after primary chemotherapy for disseminated nonseminomatous germ cell tumors: prognostic factors and role of postsurgery chemotherapy—results from an international study group. *J Clin Oncol*, 19(10): 2647-2675.

FOLKMAN J (2007) Angiogenesis: an organizing principle for drug discovery? *NAT Rev Drug Discov*, 6(4): 273-286.

FORQUER JA, HARKENRIDER M, FAKIRIS AJ, TIM-MERMAN RD, CAVALIERE R, HENDERSON MA, LO SS (2007) Brain metastasis from non-seminomatous germ cell tumor of the testis. *Expert Rev Anitcancer*

Ther, 7(11): 1567-1580.

FRIEDLANDER TW, RYAN CJ, SMALL EJ, TORTI F (2015) Testicular Cancer. In: Clinical Gate – Hematology, Oncology and Palliative Medicine. Available at: https://clinicalgate.com/testicular-cancer-2/

GHAZARIAN AA, TRABERT B, GRAUBARD BI, SCHWARTZ SM, ALTEKRUSE SF, MCGLYNN KA (2015) Incidence of testicular germ cell tumors among US men by census region. *Cancer*, 121(23): 4181-4189.

GUPTA SA, HOROWITZ JM, BHALANI SM, CHALIAN H, HAMMOND NA, BERGGRUEN S, NIKOLIADIS P, CASALINO DD (2014) Asymmetric spermatic cord vessel enhancement on CT: a sign of epididymitis or testicular neoplasm. *Abdom Imaging*, 39(5): 1014-1020.

GURNEY J, SHAW C, STANLEY J, SIGNAL V, SARFATI D (2015) Cannabis exposure and risk of testicular cancer: a systematic review and meta-analysis. *BMC Cancer*, 15: 2-10.

HANNA NA, EINHORN LH (2014) Testicular cancer – discoveries and updates. *N Eng J Med*, 371: 2005-2016.

HU B, DANESHMAND S (2015) Role of extraretroperitoneal surgery in patients with metastatic germ cell tumors. *Urol Clin N Am*, 42: 369-380.

KARESEN R, WIST E (2005) Cancer Diseases - A basic book for health professionals. 2nd edition. Gyldendal Norske Forlag, Oslo, pp 237-242.

KATO N, TAMURA G, FUKASE M, SHIBUYA H, MOTOYMA T (2003) Hypermethylation of the RUNX3 gene promoter in testicular yolk sac tumor of infants. *Am J Pathol*, 163(2): 387-391.

KESLER KA (2002) Surgical techniques for testicular nonseminomatous germ cell tumors metastatic to the mediastinum. *Chest Surg Clin N Am*, 12(4): 749-768.

LEMAN ES, GONZLGO ML (2010) Prognostic features and markers for testicular cancer management. *Indian J Urol*, 26(1): 76-81.

LOOIJENGA LHJ, OOSTERHUIS W (1999) Pathogenesis of testicular germ cell tumours. *Rev Reprod*, 4(2): 90-100.

LOTAN TA (2015) Chapter 21, The lower urinary tract and male genital system. In: *Pathologic Basis of Disease*, 9th ed., Elsevier Suanders, pp 959-989.

MARTIN TA, YE L, SANDERS AJ, LANE J, JIANG WG (2013) Cancer invasion and metastasis: molecular and cellular perspective. In: Madame Curie Bioscience Database. Available at: https://www.ncbi.nlm.nih.gov/books/NBK164700/

MASTERSON TA, SHAYEGAN B, CARVER BS, BAJORIN DF, FELDMAN DR, MOTZER RJ, BOSL GJ, SHEINFELD J (2012) Clinical impact of residual extraretroperitoneal masses in patients with advanced nonseminomatous germ cell testicular cancer. *Urology*, 79(1): 156-159.

MCGLYNN KA, TRABERT B (2012) Adolescent and adult risk factors for testicular cancer. *Nat Rev Urol*, 9(6): 339-349.

MEDICI D, HAY ED, OLSEN BR (2008) Snail and Slug promote epithelial-mesenchymal transition through beta-catenin-T-cell factor-4-dependent expression of transforming growth factor- beta3. *Mol Biol Cell*, 19(11): 4875-4887.

MILOSE JC, FILSON CP, WEIZER AZ, HAFEZ KS, MOTGOMERY JS (2012) Role of biochemical markers in testicular cancer: diagnosis, staging, and surveillance. *J Urol*, 4: 1-8.

NAGASAWA M, JOHNIN K, HANADA EIKI, YOSHIDA T, OKAMOTO K, OKADA Y, UEBA TO, TAGA T, OHTA S, KAWAUCHIH A (2015) Advanced childhood testicular yolk sac tumor with bone metastasis: a case report. *Urology,* 85(3): 671-673.

NATIONAL CANCER INSTITUTE (2017) PDQ® Testicular Cancer Treatment. Bethesda, MD: National Cancer Institute. Date last modified 01/26/2017. Available at: https://www.cancer.gov/types/testicular/hp/testicular-treatment-pdq#section/all Accessed 06/15/2017. https://www.cancer.gov/types/testicular/hp/testicular-treatment-pdq

OHYAMA C, CHIBA Y, YAMAZAKI T, ENDOH M, HOSHI S, ARAI Y (2002) Lymphatic mapping and gamma probe guided laparoscopic biopsy of sentinel lymph node in patients with clinical stage I testicular tumor. *J Urol*, 168(4 Pt 1): 1390-1395.

ONO M, TORISU H, FUKUSHI J, NISHIE A, KUWANO M (1999) Biological implications of macrophage infiltration in human tumor angiogenesis. *Cancer Chemother Pharmacol*, 43 (Suppl): S69-71.

PANDYA NM, DHALLA NS, SANTANI DD (2006) Angiogenesis--a new target for future therapy. *Vascul Pharmacol*, 44(5): 265-274.

PEINADO H, OLMEDA D, CANO A (2007) Snail, Zeb and bHLH factors in tumour progression: an alliance against the epithelial phenotype? *Nat Rev Cancer*, 7(6): 415-428.

PETTERSSON A, RICHARDI L, NORDENSKJOLD A, KAIJSER M, AKRE O (2007) Age at surgery for undescended testis and risk of testicular cancer. *N Eng J Med*, 356: 1835-1841.

POTENTE M, GERHARDT H, CARMELLIEF P (2011) Basic and therapeutic aspects of angiogenesis. *Cell*, 146(6): 873-887.

RAJPERT-DE MEYTS E, SKAKKEBAEK NE, TOPPARI J (2013) Testicular cancer pathogenesis, diagnosis and endocrine aspects. In: Endotext, Available at: https://www.ncbi.nlm.nih.gov/books/NBK278992/

SESTERHENN IA, DAVIS JR CK (2004) Pathology of germ cell tumors of the testis. *Cancer Control*, 11(5): 374-387.

SHEIKINE Y, GENEGA E, MELAMED J, LEE PENG, REUTER VE, YE H (2012) Molecular genetics of testicular germ cell tumors. *Am J Cancer Res*, 2(2): 153-167.

SILTANEN S, ANTTORNEN M, HEIKKILA P, NAOKO NARITA, LAITINEN M, RITVOS O, WILSON DB, HEIKINHEIMO M (1999) Transcription factor GATA-4 is expressed in pediatric yolk sac tumors. *Am J Pathol*, 155(6): 1832-1839.

SILVAN U, DIEZ-TORRE A, BONILLA Z, MORENO P, DIAZ-NUNEZ M, ARECHAGA J (2015) Vasculogene-

sis and angiogenesis in nonseminomatous testicular germ cell tumors. *Urol Oncol*, 33(6): 268.e17-268.e28.

SKAKKEBAEK NE, RAJPERT-DE MEYTS E, JORGENSEN N, MAIN KM, LEFFERS H, ANDERSSON AM, JUUL A, JENSEN TK, TOPPARI J (2007) Testicular cancer trends as 'whistle blowers' of testicular developmental problems in populations. *Int J Androl*, 30(4): 198-204.

SKAKKEBAEK NE, RAJPERT-DE MEYTS E, MAIN KM (2001) Testicular dysgenesis syndrome: an increasingly common developmental disorder with environmental aspects. *Hum Reprod*, 16(5): 972-978.

STEVENSON SM, LOWRANCE WT (2015) Epidemiology and diagnosis of testis cancer. *Urol Clin N Am*, 42: 269-275.

SULEYMAN N, MOGHUL M, GOWRIE-MOHAN S, LANE T, VASDEV N (2016) Classification, epidemiology and therapies for testicular germ cell tumours. *J Genit Syst Disor*, S2(0)(2): 1-3.

TALARICO JR EF (2010) A human dissection training program at Indiana University School of Medicine-Northwest. *Anat Sci Educ*, 3(2): 77-82.

TALARICO JR EF (2013) A change in paradigm: giving back identity to donors in the anatomy laboratory. *Clin Anat*, 26(2): 161-172.

TALERMAN A (1980) Endodermal sinus (yolk sac) tumor elements in testicular germ-cell tumors in adults: comparison of prospective and retrospective studies. *Cancer*, 46(5): 1213-1217.

THE AMERICAN JOINT COMMITTEE ON CANCER (2010) Cancer Staging Manual, 7th edition, pp 470-471.

THIERY JP (2002) Epithelial-mesenchymal transitions in tumour progression. *Nat Rev Cancer*, 2(6): 442-454.

TRABERT B, CJEM K, DEVESA SS, BRAY F, MCGLYNN KA (2015) International patterns and trends in testicular cancer incidence, overall and by histological subtype, 1973-2007. *Andrology*, 3(1): 4-12.

VASDEV N, MOON A, THORPE AC (2013) Classification, epidemiology and therapies for testicular germ cell tumours. *Int J Dev Biol*, 57(2-4): 133-139.

WOLDU SL, MCKIEMAN JM (2015) Reoperative retroperitoneal surgery: etiology and clinical outcomes. *Urol Clin North Am*, 42(3): 381-392.